

Uncertainty Budget of Version 2 Data from Summit

The uncertainty of Version 2 data from the SUV-150B spectroradiometer at Summit is composed of uncertainties related to (i) radiometric calibration; (ii) instability of instrument responsivity; (iii) cosine and azimuthal errors; (iv) the finite resolution of the spectroradiometer; (v) residual wavelength errors after wavelength correction; (vi) non-linearity; (vii) stray light and fluorescence; and (viii) photon and electronic noise. The different error sources will be analyzed in detail below. The procedure is based on theoretical consideration described by *Bernhard et al.* [1999]. The same method has also been applied to measurements from SUV-100 instruments located at the South Pole [*Bernhard et al.*, 2004], McMurdo [*Bernhard et al.*, 2006b], Palmer [*Bernhard et al.*, 2005a], and Barrow [*Bernhard et al.*, 2007].

1. Radiometric calibration

Uncertainties related to the radiometric calibration are summarized in Table 1 and explained below.

1.1. Standards of Spectral Irradiance

Calibrations of the SUV-150B spectroradiometer at Summit between August 2004 and July 2007 were performed with two 200-Watt tungsten halogen lamps of type Q6.6AT4/5CL from General Electric. The lamps had been calibrated in 2001 by Optronic Laboratories Inc. (OLI) against 1000-Watt standards of spectral irradiance of type FEL. The calibration of these FEL standards is traceable to the National Institute of Standards and Technologies (NIST) source-based spectral irradiance scale from 1990 (“NIST1990” scale). The expanded uncertainty (coverage factor $k=2$) of this scale is 1.8% at 250 nm, 1.1% at 350 nm, and 0.9% at 655 nm [*Walker et al.*, 1987]. According to OLI calibration reports, the transfer of the calibration from NIST FEL standards to 200-Watt lamps involves an additional uncertainty of 1.1% between 250 and 350 nm, and 0.8% between 350 and 650 nm.

In 2000, NIST produced a new detector-based irradiance scale (“NIST2000 scale”) [*Yoon et al.*, 2002]. If solar measurements of the Summit instrument had been based on this scale, spectral irradiance would be higher by approximately 1.5% at 300 nm, 1.1% at 400 nm, and 0.8-1% in the visible.

Prior to their use at Summit, the two 200-Watt lamps were also compared to four FEL lamps provided by the U.S. Central UV Calibration Facility (CUCF; <http://www.srrb.noaa.gov/calfacil/cucfhome.html>). These lamps are traceable to the NIST2000 scale. When the lamps’ calibrations were scaled to the NIST1990 scale, they agreed to within $\pm 0.5\%$ with the OLI calibration of the 200-Watt lamps, confirming the OLI irradiance scale.

When the two 200-Watt lamps were again compared with the CUCF lamps in 2007, their calibration was low by $2\pm 0.5\%$, indicating that the lamps had drifted during their tenure at Summit. The lamps were recalibrated and the calibration of solar data from 2007 refers to the new calibration. However, the temporal pattern of the drift is not clear. Solar from 2004-2006 refer to the original OMI calibration. Solar data from 2005-2006 are likely biased low by 1-2%.

1.2. Calibration Procedure

The 200-Watt lamps are operated within a cylindrical barrel with a blackened inner wall that mounts atop the instrument [Bernhard *et al.*, 2006a]. Measurements indicate that stray light from diffuse reflections either from the barrel or lamp holder is between 0.1 and 0.3% of the measured signal. The nominal distance between the standard and the instrument's collector is 50 cm. The uncertainty of the distance is 1.0 mm, causing a 0.4% uncertainty in irradiance. Uncertainties due to other alignment errors are likely smaller than 0.2% [Bernhard and Seckmeyer, 1999]. The air within the barrel is not temperature stabilized. Calibrations in an environmental chamber at 30°C and –20°C did not show a significant temperature dependence.

200-Watt lamps are operated at a current of 6.5 A. The current is monitored with high-accuracy shunts and voltmeters, which are frequently recalibrated. The uncertainty of the current measurement is 0.05%, which leads to an irradiance uncertainties of 0.5% at 300 nm and 0.25% at 600 nm. The lamp power supply is digitally controlled and the output current can only be adjusted in steps of 0.0044 A, leading to an additional uncertainty of 0.3% at 300 nm and 0.1% at 600 nm.

Values stated in OLI calibration reports are specified in 10 nm steps. We interpolated these values to intermediate wavelengths by fitting a Planck function to the data points. This fit method leads to uncertainties of about 0.5% (see [Bernhard *et al.*, 2006a]) as actual lamp spectra deviate from a Planck function.

Table 1. Standard uncertainty ($k=1$) of radiometric calibration.

Error Source	Uncertainty in %		
	310 nm	400 nm	600 nm
NIST spectral irradiance scale from 1990	0.7	0.5	0.5
Transfer from NIST FEL lamps to OLI 200-Watt lamps	0.5	0.4	0.4
Drift of 200-Watt site standards	1.5	1.5	1.5
Stray light in calibration setup	0.2	0.2	0.2
Distance 200-Watt lamp – collector SUV-100	0.4	0.4	0.4
Alignment errors	0.2	0.2	0.2
Calibration shunt and voltmeter for lamp current measurement	0.5	0.3	0.2
Resolution power supply during 200-Watt lamp scans	0.3	0.2	0.1
Interpolation calibration certificates	0.5	0.5	0.5
Combined uncertainty of radiometric calibration	2.0	1.8	1.8

2. Stability of SUV-150B responsivity

The responsivity of the SUV-150B changed by large amounts during the operational period at Summit (August 2004 – July 2007). During August and December 2004, the responsivity decreased by up to 25-32% in the UV-B, 7-25% in the UV-A, and 2-7% in the visible. The system's sensitivity partly recovered during the following months. Between January and May 2005, the responsivity increased by up to 20% in the UV-B, 20-27% in the UV-A, and the 0-20% in visible [Bernhard *et al.*, 2006a]. The large sensitivity changes were mostly caused by rapid degradation (“yellowing”) of the internal coating of the integrating sphere that is part of the instrument's fore optics. Since the rate of change was monotonic and predictable,

the drift could be corrected by linear interpolation between bi-weekly calibrations with the 200-Watt standards.

In response to the problem, the original integrating sphere, which was coated with Barium sulfate, was replaced in August 2005 by a new sphere made from solid shells of Polytetrafluoroethylene (PTFE). The throughput of the new sphere was stable at the $\pm 4\%$ level between August 2005 and May 2006. Between May and December 2006, the throughput decreased monotonically by about 20% at 320 nm, 15% at 340 nm and less than 5% in the visible (Volume 15 Network Operations Report, in preparation). There were also changes in system responsivity not related to the integrating sphere in the order of 15% between February and September 2006. The reasons of these drifts are currently not known, but all changes were progressing predictably over time, and could be corrected by frequently adjusting the instrument's calibration.

SUV-150B data were compared with measurements of the co-located GUV-511 multi-channel radiometer to confirm that changes in responsivity have been corrected appropriately. For this comparison, SUV-150B spectra were weighted with the measured response functions of the GUV-511 as described by *Bernhard et al.* [2005b]. The analysis is complicated by the fact that the responsivity of the GUV-511 also changed over time. Between May 2004 and July 2007, the sensitivity of the GUV decreased monotonically by 19% at 320 nm, 7% at 340 nm, and 10% at 380 nm. To decouple the drifts of the two instruments, we calibrated the GUV-511 radiometer against corrected SUV-150B data using synchronous measurements collected during periods ranging from three to five months. Drifts of the GUV's 340 and 380 nm channels during these short periods are smaller than 1.5%. GUV data are therefore a suitable reference for detecting drifts in SUV-150B data between the bi-weekly calibration events. The method blends the strengths of both instruments: the responsivity of the SUV-150B is accurately known at the times of calibrations, and the good short-term stability of the GUV-511 allows the assessment of drifts.

Figure 1 shows the ratio of SUV-150B and GUV-511 measurements for 6 different periods. The ratios show discontinuities of up to 3% at times when the calibration of the SUV-150B was changed, but the overall agreement is good. Table 2 shows the standard deviations of the ratios of SUV/GUV for all periods and wavelengths. Standard deviations range between 0.011 and 0.022; the average standard deviation is 0.015. These small values confirm that changes in responsivity of the SUV-150B have been correctly adjusted. Based on this analysis, a standard uncertainty of 2% is associated with the instability of the SUV-150B responsivity. Note that this is a conservative estimate since the uncertainty measure is somewhat inflated by the small drifts of the GUV-511 radiometer during the comparison periods.

It has been noted recently that the transmission of PTFE diffusers changes with temperature [*McKenzie et al.*, 2005]. The largest transmission change of 2% occurs between 10 °C and 20 °C. There is virtually no change above 20 °C. The temperature of the SUV-150B's integrating sphere is maintained at 32 ± 5 °C. No uncertainty was associated with this effect.

Table 2. Standard Deviation of Ratio of SUV-150B and GUV-511 Measurements.

Data Volume	Period	Standard Deviation		
		320 nm	340 nm	380 nm
14	August 2004 – October 2004	0.015	0.014	0.022
14	February 2005 – May 2005	0.016	0.019	0.018
15	August 2005 – October 2005	0.013	0.010	0.012
15	February 2006 – June 2006	0.015	0.012	0.017
15	June 2006 - October 2006	0.016	0.012	0.019
16	February 2007 – July 2007	0.011	0.012	0.017
Average		0.014	0.013	0.017

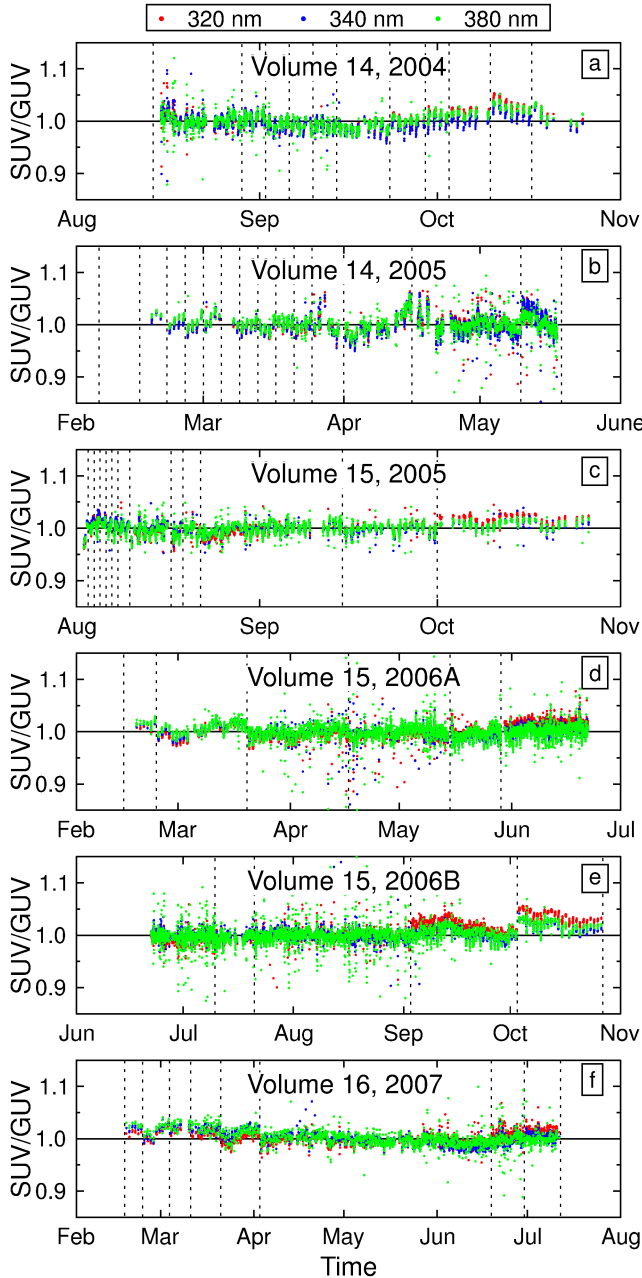


Figure 1: Ratio of SUV-150B and GUV-511 at 320, 340, and 380 nm for six periods using data with solar zenith angles smaller than 85°. Vertical broken lines indicate times when the calibration of the SUV-150B was changed.

Panel a: August 2004 – November 2004.
 Panel b: February 2005 – June 2005.
 Panel c: August 2005 – November 2005.
 Panel d: February 2006 – July 2006.
 Panel e: June 2006 – Nov 2006.
 Panel f: February 2007 – August 2007.

3. Uncertainties caused by the cosine error

Uncertainties caused by the cosine error were calculated according to *Bernhard et al.* [2004]. Input parameters and results of the calculation are presented in the following.

3.1. Nomenclature

SZA or θ	Solar zenith angle in degrees
λ	Wavelength in nm
f_B	Cosine error, expressed as ratio of actual and ideal cosine response
$u_R(f_B)$	Relative uncertainty of cosine error
f_D	Diffuse cosine error, defined as the error in measuring isotropic radiance
$u_R(f_D)$	Relative uncertainty of f_D
R	Ratio of irradiance from the direct solar beam on a horizontal surface to global irradiance
$u_R(R)$	Relative uncertainty of R
f_G	Ratio of measured global irradiance affected by the cosine error to true global irradiance
$u_R(f_G)$	Relative uncertainty of f_G
τ	Cloud optical depth at 450 nm
$\tau_A(\lambda)$	Aerosol optical depth at wavelength λ

3.2. Determination of cosine error and its uncertainty

The cosine error f_B of the SUV-150B spectroradiometer was measured prior to deployment in BSI's calibration laboratory. Measurements were performed at azimuth angles of 0°, 90°, 180°, and 270°, and at wavelength of 320, 350, 400, 500, and 600 nm. There were no systematic differences for the different azimuth angles and wavelengths. Figure 1 shows the average cosine error f_B of the original Barium-sulfate coated integrating sphere. Errors bars indicate the standard deviation of σ_f calculated from the measurements at different azimuth angles and wavelengths. The cosine error is smaller than 2% for incidence angles up to 75°, -6% at 80°, and 1.5% for isotropic illumination. The relative error of the cosine error, $u_R(f_B)$, is defined as σ_f / f_B .

The cosine error of the new PTFE integrating sphere could not be tested. Although the physical dimensions of the new and original spheres are identical, different reflection properties of the two material may lead to different cosine errors. To further investigate this possibility, we compared Version 2 measurement and model results for clear-sky situations. Figure 2 shows the ratio of clear-sky measurements at 360, 400, 500, and 590 nm to the associated model results as a function of solar zenith angle (SZA). Data collected between 15-August 2004 and 17-May 2005 using the original sphere are indicated by red dots; data collected between 17-August 2005 and 4-December 2005 with the new sphere are shown with blue dots. Data of both periods were also normalized to the median of ratios calculated for the SZA-range 59°-61° to remove small (<±2.5%) difference between the two period, which were likely caused by the instrument's calibration. Figure 2 demonstrates that there is no systematic difference of the ratios between the SZA-range of 60°-80°. The small upward slope visible at 400 and 500 nm is present in both data sets. The good agreement indicates that the cosine error of the system did not appreciably change when the sphere was replaced. Assessment of the consistency of the two spheres beyond 80° is difficult. We therefore doubled the uncertainty $u_R(f_B)$ for SZA=80° and 85° to 2.7% and 4.6%, respectively.

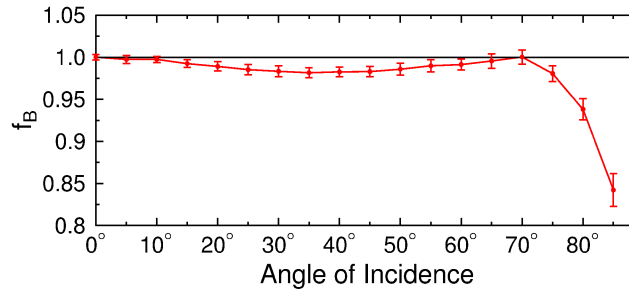


Figure 2: Cosine error of SUV-150B equipped with the original Barium-sulfate coated integrating sphere. Error bars indicate the standard deviation of measurements at different azimuth angles and wavelengths.

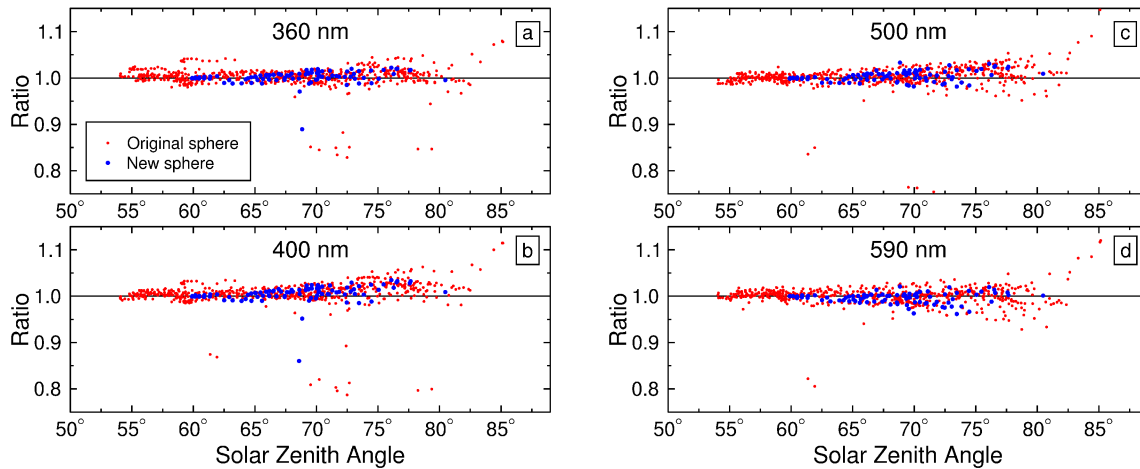


Figure 3: Ratio of measured and model clear-sky spectral irradiance at 360 nm (Panel a), 400 nm (Panel b), 500 nm (Panel c), and 590 nm (Panel d). Data from the period when original (new) sphere was installed are indicated by red (blue) dots. Data were normalized to the median ratio of the SZA-range 59°-61°. Clear-sky classification is based on the variability of spectral irradiance at 600 nm. Outliers at 360 and 400 nm are likely caused by incorrect clear-sky assignment.

3.2. Calculation of uncertainties caused by the cosine error

SUV-150B data were corrected for the cosine error by multiplication with the correction factor $1/f_G$, where $f_G(\theta, \lambda) = f_B(\theta, \lambda) R(\theta, \lambda) + f_D(\lambda) [1 - R(\theta, \lambda)]$, see [Bernhard *et al.*, 2004]. In addition to f_B , the calculation of $f_G(\theta, \lambda)$ requires the ratio of direct/global irradiance $R(\theta, \lambda)$, which is estimated from model calculations. The largest uncertainty in estimating $R(\theta, \lambda)$ stems from the uncertainty of aerosol optical depth (AOD) used as input to the model. Measurements of aerosol optical depth are not available for Summit. Calculations were performed for background aerosol conditions and parameterized with Ångström's turbidity formula. The Ångström parameters α and β were set to 1.0 and 0.008, respectively. This translates to an aerosol optical depth of $\tau_A(500\text{nm})=0.015$. This value is about the lowest aerosol optical depth that can be expected at Summit. During most of the time, the actual AOD may

be larger, and the ratio of direct/global irradiance will therefore be lower than calculated. However, increased AOD will also lead to reduced global irradiance, which is interpreted as an optical thin cloud by the algorithm, and the modeled ratio $R(\theta, \lambda)$ is adjusted accordingly [Bernhard *et al.*, 2004]. The uncertainty of this approach is small since thin clouds lead to a similar change in $R(\theta, \lambda)$ than a aerosol layer. The uncertainty is mostly caused by the fact that the algorithm for calculating cloud optical depth τ has to allow for some variability in the calibration of SUV-150B measurements. For example, when measured irradiance at 450 nm is low by up to 2%, the algorithm still assumes clear sky conditions and model calculations will be based on AOD of $\tau_A(500\text{nm}) = 0.015$ cloud optical depth of $\tau = 0$. A reduction of global irradiance at 450 nm by 2% requires an optical depth of 0.05 at SZA=70° and 0.024 at SZA=80°. Based on these considerations, the relative uncertainty $u_R(R)$ of the direct/global ratio was estimated by modeling $R(\lambda)$ for $\tau_A(500\text{nm}) = 0$ and $\tau_A(500\text{nm}) = 0.05$, and calculating the difference. These calculations result in the following values for $u_R(R)$: $u_R(R) = 4\%$ at SZA=40°, 7% at SZA=65°, 16% at SZA=80°, and 35% at SZA=85°.

The uncertainty $u_R(f_D)$ of the diffuse cosine error f_D is mostly caused by the assumption that sky radiance is isotropic. It was estimated as described by Bernhard *et al.* [2004] by comparing calculations for isotropic distributions with model calculations of sky radiance distributions for a variety of atmospheric conditions and surface albedo.

Table 3 summarizes the uncertainty of the cosine error correction, $u_R(f_G)$, for a variety of SZAs, wavelengths, and cloud optical depths. Uncertainties for SZA ≤ 70° are smaller than 1.1%. The small values can be attributed to the fact that the cosine error of the SUV-150B collector is small. At SZA=85°, uncertainties range between 0.5% and 5.3%. The largest uncertainty applies at 600 nm during conditions of variable cloudiness (“ $\tau=?$ ”), when it is not possible to determine whether or not the disk of the Sun is visible.

The ratio of measured at modeled global irradiance does not exhibit any systematic difference for morning and afternoon data, confirming that the collector has no noticeable azimuthal error and that the instrument was well leveled. However, a small azimuthal error may still exist even though it cannot be detected due to variability in the data. The upper limit for the uncertainty due to azimuthal variations is 0.35% at 600 nm and SZA=75°. The uncertainty decreases with decreasing wavelength and SZA, and is 0.2% in the UV.

Table 3. Standard Uncertainty (k=1) Caused by the Cosine Error as a Function of SZA, Wavelength λ and Cloud Optical Depth τ .

SZA [deg]	λ [nm]	f_B	f_D	R	$\tau = 0$			$\tau = 0.2$			$\tau = 1.0$		$\tau = ?$
					f_G	$u_R(f_G)$	R	f_G	$u_R(f_G)$	R	f_G	$u_R(f_G)$	$u_R(f_G)$
60	310	0.99	0.984	0.32	0.986	0.4%	0.22	0.986	0.4%	0.05	0.984	0.5%	0.7%
60	400	0.99	0.984	0.62	0.988	0.5%	0.42	0.987	0.4%	0.09	0.985	0.5%	0.8%
60	600	0.99	0.984	0.90	0.990	0.6%	0.62	0.988	0.5%	0.14	0.985	0.5%	0.9%
70	310	1.00	0.984	0.17	0.987	0.5%	0.10	0.986	0.5%	0.01	0.984	0.5%	0.7%
70	400	1.00	0.984	0.53	0.993	0.5%	0.32	0.989	0.5%	0.03	0.985	0.5%	0.8%
70	600	1.00	0.984	0.87	0.998	0.8%	0.53	0.993	0.5%	0.06	0.985	0.5%	1.1%
80	310	0.94	0.984	0.01	0.984	0.5%	0.00	0.984	0.5%	0.00	0.984	0.5%	0.8%
80	400	0.94	0.984	0.32	0.969	1.0%	0.11	0.979	0.6%	0.00	0.984	0.5%	1.2%
80	600	0.94	0.984	0.79	0.948	2.2%	0.32	0.970	1.0%	0.00	0.984	0.5%	2.5%
85	310	0.84	0.984	0.00	0.984	0.5%	0.00	0.984	0.5%	0.00	0.984	0.5%	0.8%
85	400	0.84	0.984	0.11	0.969	0.9%	0.01	0.982	0.6%	0.00	0.984	0.5%	1.1%
85	600	0.84	0.984	0.65	0.892	4.6%	0.10	0.970	0.8%	0.00	0.984	0.5%	5.3%

“ $\tau = ?$ ” indicates scattered-cloud conditions.

4. Spectral Resolution

The slit function of the SUV-150B is shown in Figure 4. The bandwidth is 0.63 nm full width at half maximum (FWHM). The finite bandwidth leads to an overestimation of the solar spectrum in the UV-B. This effect has been discussed by *Bernhard and Seckmeyer* [1999], and their results are adopted here. For the SUV-150B, spectral irradiance at 305 nm is overestimated by less than 1%. The effect is generally insignificant for wavelengths above 310 nm. However, at wavelengths at the detection limit (0.0001 $\mu\text{W}/(\text{cm}^2 \text{ nm})$, see Section 8), the overestimate can be as large as 8%. For example, at SZA=40° and total ozone of 400 DU, the smallest wavelength with detectable signal is at 294.2 nm, and the overestimate is approximately 7%. Measurements of erythemal irradiance (action spectrum by *McKinlay and Diffey*, [1987]) are overestimated by less than 0.15%. The error for DNA-damaging irradiance (action spectrum by *Setlow* [1974]) is 0.4%. The effect of the finite bandwidth is therefore negligible for most practical applications. The finite resolution of the SUV-100 also leads to “smoothing” of the Sun’s Fraunhofer lines. We did not associate an uncertainty to this effect.

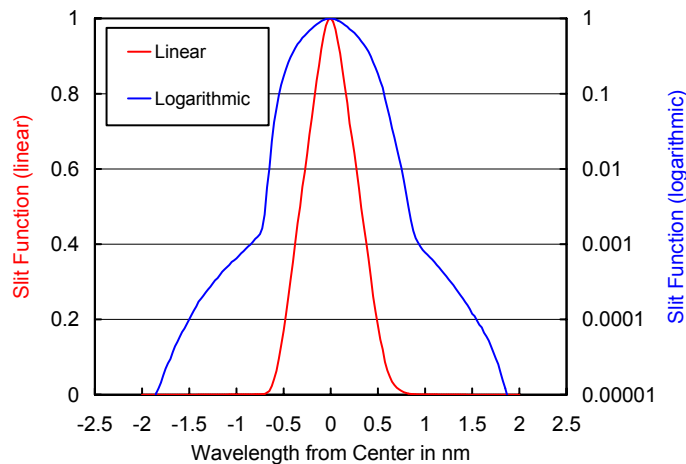


Figure 4: Slit function SUV-150B, measured with a Helium-Cadmium laser at 325 nm.

5. Wavelength Misalignment

The wavelength precession of the SUV-150B is better than ± 0.01 nm ($\pm 1\sigma$) [Bernhard *et al.*, 2006a]. The good stability is due to the use of high-resolution optical encoders, which provide feedback control of the instrument's stepper motors. The wavelength accuracy of spectra was checked with the Version 2 correlation algorithm described by Bernhard *et al.* [2004]. The reference spectrum of this method refers to the refractive index at sea level. Residual wavelength errors are ± 0.008 nm ($\pm 1\sigma$) in the UV-A, ± 0.009 nm between 400 and 500 nm, and 0.013 nm between 500 and 600 nm. The actual wavelength uncertainty of the system is larger than these number due to uncertainties of the check-algorithm of approximately 0.01 nm. The total wavelength uncertainty was calculated by combining the two components in quadrature. It is 0.013 nm between 300 and 500 nm and 0.016 nm between 500 and 600 nm.

We implemented Eq. (26) of [Bernhard and Seckmeyer, 1999] to translate wavelength uncertainties in the ozone cutoff region of the solar spectrum to irradiance uncertainties. Resulting standard uncertainties for irradiance are 0.8% at 305 nm, 0.5% at 310 nm, <0.2% for wavelengths above 320 nm, and about 0.2% for erythemal irradiance and 0.5% for DNA-damaging irradiance.

Interaction of wavelength shifts with the Fraunhofer structure of the solar spectrum leads to an additional uncertainty. This uncertainty was calculated by shifting the extraterrestrial spectrum by 0.014 nm (i.e. the approximate wavelength uncertainty of SUV-150B spectra), and applying Eq. (25) of [Bernhard and Seckmeyer, 1999] to the ratio of shifted to unshifted spectrum. The resulting uncertainties are 0.4% between 300 and 380 nm, 0.8% between 390 and 400 nm (the range of the strong Calcium Fraunhofer lines), and approximately 0.1% in the visible, where the Fraunhofer structure is less pronounced compared to the UV.

6. Non linearity

The detector of the SUV-150B is a photomultiplier tube (PMT) from Hamamatsu (Model R2371P) with a maximum rated anode current of 10 μ A. It is operated at an anode current of up to 1 μ A. The manufacturer does not provide a linearity specification. The current is amplified with a electrometer from Keithley (Model 6514), which is linear to within $\pm 0.2\%$ over the wavelength range 0.001 to 2 μ A according to the manufacturer.

The uncertainty of SUV-150B measurements caused by non-linearity was tested by comparing SUV-150B and GUV-511 data. If both systems are linear, the ratio of their readings should not depend on irradiance. Figure 5 shows the ratio of SUV-150B and GUV-511 for data measured between 21-July 2006 and 1-September 2006. Both instruments were stable during this period to better than $\pm 1\%$ (Figure 1e). The ratio of SUV/GUV is plotted against the ratio of solar irradiance to the irradiance during calibration, denoted R_i . Thus, $R_i = 1$ on the abscissa of Figure 5 means that the Sun produced the same irradiance on the instrument's collector than the calibration lamp. Ratios are plotted for the wavelengths of 320, 340, and 380 nm. In order to homogenize results from the three wavelengths, the ratios were normalized to the median of ratios from the range $9 < R_i < 10$. Normalization factors range between 0.990 and 1.003.

Figure 5 indicates that the ratio of SUV/GUV typically varies 0.98 and 1.02; the standard deviation is 0.009 for all wavelengths. The average ratio increases from about 1.0 at $R_1=100$ to 1.014 at $R_1=250$. This increase could be due a non-linear behavior of the photomultiplier [Bernhard and Seckmeyer, 1999]. There are also discontinuities between $R_1=1$ and $R_1=5$. These can be related to gain-changes of the GUV-511 radiometer. Based on these considerations, we set the standard uncertainty of SUV-150B measurements caused by non-linearity to 0.9% for small and 0.4% for large SZAs. Note that this is a conservative estimate since some of the patten in Figure 5 is due to the GUV-511, and some variation is also introduced by changes in responsivity of the two instruments.

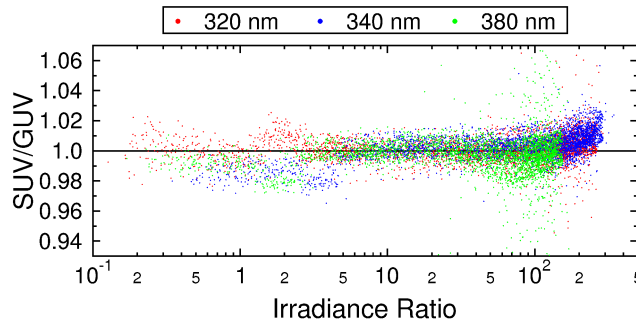


Figure 5: Ratio of SUV-150B and GUV-511 measurements recorded between 21-July 2006 and 1-September 2006 as a function of the irradiance ratio R_1 for 320, 340, and 380 nm. R_1 is defined as the ratio of solar irradiance and the irradiance of the calibration lamp.

7. Out-of-band Rejection, Fluorescence, and Stray Light

Out-of-band rejection of the SUV-150B monochromator was determined by measuring the line of a Helium Cadmium laser at 325 nm. Figure 6 indicates that out-of-band rejection is at least $5 \cdot 10^8$, which was the maximum dynamic range achievable with the test setup. The true out-of-band rejection is likely larger, but this could not be proven. Figure 6 also shows fluorescence of the integrating sphere's material caused by excitation from the laser line. Fluorescence is smaller than $1 \cdot 10^{-5}$ and therefore of no relevance for solar measurements. Note that measurements were performed with the Barium-sulfate coated sphere. The new PTFE sphere was not examined for fluorescence. However, our measurements with other PTFE samples indicated that the fluorescence of PTFE is smaller than that of Barium-sulfate coating. Uncertainties due to fluorescence are therefore negligible.

Stray light stems from photons with wavelengths outside the wavelength range of the monochromator's slit function that are detected together with photons inside this range. For processing of solar spectra, the average of PMT currents measured between 280 and 290 nm is routinely subtracted from the PMT current at larger wavelengths. If the contribution from stray light were independent of wavelength, no uncertainty would apply. Stray light becomes only a source of error if it changes with wavelength.

The system was tested for stray light based on the fact that solar radiation below 290 nm is completely filtered by the ozone layer. If no stray light is present, PMT signals at wavelengths below 290 should be independent of time of day. If the stray light suppression of the monochromator is imperfect, PMT signals below 290 nm should increase with solar radiation levels and be highest at noon. To quantify a possible

stray light contribution, the average PMT signal for wavelengths between 280 and 290 nm was calculated from every spectrum recorded in 2007. These average PMT signals are denoted the spectrum's "offset" in the following. For every day, the spectrum with the largest SZA was determined. The associated average PMT signal is the night-time offset of the given day. This offset can obviously not be affected by stray light and represents the true PMT dark current. The night-time offset was subtracted from the offsets measured during the day for quantifying the systematic diurnal variation of the PMT offset. The difference of day and night offsets is plotted in Figure 7a as a function of spectral irradiance at 600 nm. The figure indicates an upward slope. The average day-night difference is equal to unity at low radiation levels, but increases to 0.06 pA for times when the spectral irradiance at 600 nm is larger than $60 \mu\text{W}/(\text{cm}^2 \text{ nm})$. This increase is indicative for stray light. However, the true cause could also be a systematic diurnal change in room temperature where the instrument is located. Some of the scatter of Figure 7a is due to drifts of the PMT's dark current not related to solar radiation levels. The possible stray light contribution has to be compared with the uncertainty in measuring the dark current. The latter was estimated by calculating the difference of the PMT offset from consecutive spectra. These differences are shown in Figure 7b. There is no dependence on solar radiation levels, as expected. The standard deviation is 0.047 pA. The standard uncertainty of a single offset measurement is therefore $0.047 / \sqrt{2} \text{ pA} = 0.033 \text{ pA}$. The upper limit of the stray light contribution of 0.06 pA is consequently $0.06 / 0.033 = 1.82$ times the uncertainty of the dark current. Since the offset is subtracted from solar measurements for determining the spectral irradiance, the small stray light contribution is negligible. To confirm this, the spectral irradiance at 285 nm was calculated from all spectra measured during the day and compared with the night-time value. The difference of day and night measurements is shown in Figure 7c. There is no dependence on solar radiation levels. The standard deviation is $0.00015 \mu\text{W}/(\text{cm}^2 \text{ nm})$.

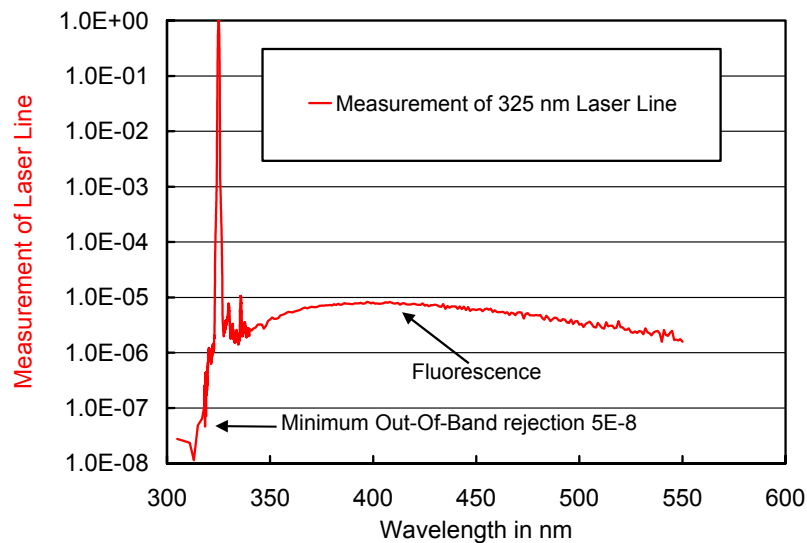


Figure 6: Measurement of the 325 nm line of a HeCd Laser for determining out-of-band rejection. Out-of-band rejection is likely larger than $5 \cdot 10^{-8}$ but this cannot be proven because the measurement is limited by the instrument's dynamical range of about 8 orders of magnitude. Fluorescence is smaller than $1 \cdot 10^{-5}$ and therefore does not affect solar measurements.

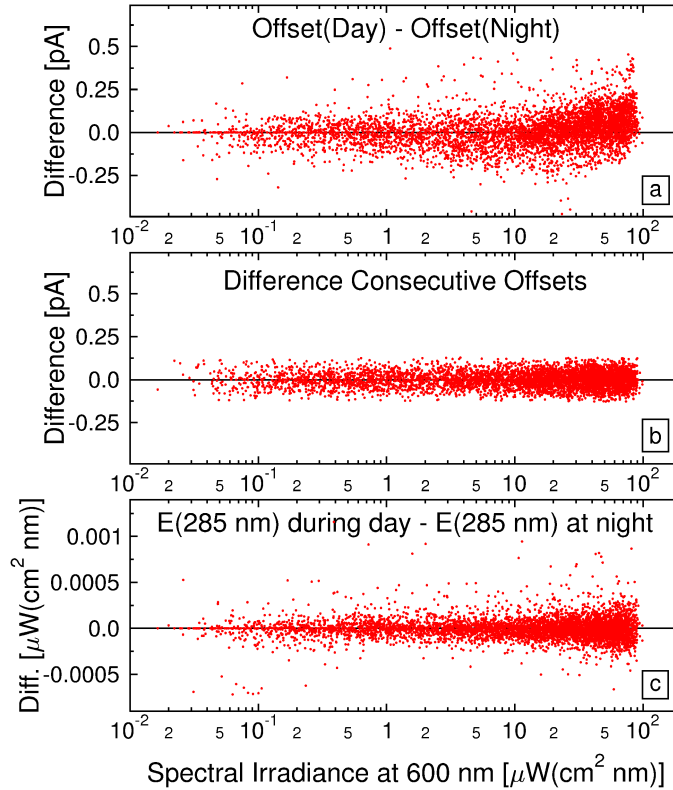


Figure 7: Determination of stray light. Panel a: Difference of PMT day and night-time offsets plotted as a function of spectral irradiance at 600 nm. The night-time offset is calculated from the daily spectrum with the largest SZA. Panel b: Difference of consecutive offset measurements. Panel c: Difference of spectral irradiance at 285 nm measured at day and night.

8. Noise and Detection Limit

During the bi-weekly calibration of the SUV-150B, the irradiance scale of one of the 200-Watt lamps is transferred to an internal 45-Watt lamp of the instrument. This lamp is scanned every day to monitor the stability of the system [Bernhard *et al.*, 2006a]. Solar spectral irradiance $E_S(\lambda)$ is calculated from the PMT current during solar scans, $I_S(\lambda)$, the PMT current during scans of the internal 45-Watt lamp, $I_{45}(\lambda)$, the PMT dark current $I_D(\lambda)$, and spectral irradiance $E_{45}(\lambda)$ assigned to the 45-Watt Lamp by:

$$E_S(\lambda) = \frac{I_S(\lambda) - I_D(\lambda)}{I_{45}(\lambda) - I_D(\lambda)} E_{45}(\lambda)$$

The relative uncertainty $u_R(E_S(\lambda))$ of $E_S(\lambda)$ due to noise in the three PMT currents is then:

$$u_R(E_S(\lambda)) = \left\{ \frac{[u(I_S(\lambda))]^2 + [u(I_D(\lambda))]^2}{[I_S(\lambda) - I_D(\lambda)]^2} + \frac{[u(I_{45}(\lambda))]^2 + [u(I_D(\lambda))]^2}{[I_{45}(\lambda) - I_D(\lambda)]^2} \right\}^{0.5},$$

where $u(I_S(\lambda))$, $u(I_{45}(\lambda))$, and $u(I_D(\lambda))$ are the uncertainties of $I_S(\lambda)$, $I_{45}(\lambda)$, and $I_D(\lambda)$, which were determined by statistical analysis. The uncertainty of $E_{45}(\lambda)$ is not considered here as it already part of the responsivity drift uncertainty. $u_R(E_S(\lambda))$ was calculated at selected wavelengths and SZAs using clear-sky spectra measured between 11-May and 15-May 2005. The ozone column during this period varied between 350 and 375 nm. Figure 8 shows $u_R(E_S(\lambda))$ as a function of wavelengths for four SZAs. $u_R(E_S(\lambda))$ is smaller than 1% for wavelengths in the UV-A and SZAs up to 85°. The uncertainty in the UV-B shows a large increase toward shorter wavelengths. At 310 nm, $u_R(E_S(\lambda))$ ranges between 0.6% for SZA=60° and 2.5% for SZA=80°. The UV-B uncertainty also depends on the ozone column (not shown). The uncertainties for erythemal (CIE weighting) and DNA-damaging irradiance were calculated with Eqs. (30) and (31) of *Bernhard and Seckmeyer* [1999]. Figure 8 indicates that the uncertainty of erythemal irradiances remains negligible for SZAs as high as 85°. The influence of noise on DNA-damaging irradiance increases sharply for SZAs larger than 80° and is 1.3% for SZA=85°.

The detection limit is defined as “noise equivalent irradiance” (NEI), and was calculated as the standard deviation of spectral irradiance at 285 nm. At this wavelength, no radiation from the Sun reaches the Earth’s surface, and the spectral irradiance reported by the instrument is only due to signal noise (see Section 7). Data analysis revealed that NEI is 0.0007 $\mu\text{W}/(\text{cm}^2 \text{ nm})$ for Volume 14 data (August 2004 – May 2005) and 0.0001 $\mu\text{W}/(\text{cm}^2 \text{ nm})$ for measurements of Volumes 15 and 16. The elevated noise level in early data is due to occurrence of electronic noise and occasional spikes in the electrometer readout, as well as the lower throughput of the integrating sphere installed during the Volume 14 period [*Bernhard et al.*, 2006a].

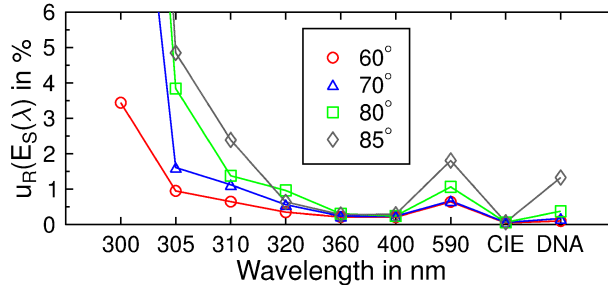


Figure 8. Relative uncertainty $u_R(E_S(\lambda))$ in solar spectral irradiance due to signal noise in calibration and solar scans. $u_R(E_S(\lambda))$ is plotted for several solar zenith angles at seven wavelengths, and for erythemal irradiance (CIE), and DNA-damaging irradiance.

9. Combined uncertainty

The combined uncertainty is presented in Table 4. Expanded relative uncertainties (coverage factor $k=2$, equal to uncertainties at the 2σ or 95.5% confidence level) vary between 5.8% and 7.4%. The uncertainty budget is dominated by uncertainties related to calibration and responsivity drifts. The uncertainty caused by the cosine error is only of importance at large wavelengths and SZAs above 80°. Expanded uncertainties for erythemal and DNA damaging irradiance vary between 5.8% and 6.2%.

Table 4. Uncertainty Budget of Version 2 Data Summit.

Error source	Relative Standard Uncertainty in %									
	SZA=65°					SZA=80°				
	310 nm	400 nm	600 nm	Ery ^a	DNA ^b	310 nm	400 nm	600 nm	Ery ^a	DNA ^b
Radiometric calibration	2.0	1.8	1.8	2.0	2.0	2.0	1.8	1.8	2.0	2.0
Responsivity drift	2.0	2.0	2.0	2.0	2.0	2.0	2.0	2.0	2.0	2.0
Cosine error ^c	0.4	0.5	0.6	0.4	0.4	0.5	1.0	2.2	0.5	0.5
Azimuthal error	0.1	0.2	0.4	0.1	0.1	0.1	0.2	0.4	0.1	0.1
Spectral Resolution	0.2	0.0	0.0	0.1	0.4	0.5	0.0	0.0	0.1	0.3
λ- shift in UV-B	0.5	0.0	0.0	0.3	0.6	0.7	0.0	0.0	0.2	0.4
λ- shift + Fraunh. lines	0.4	0.8	0.1	0.1	0.1	0.4	0.8	0.1	0.1	0.1
Non-linearity	0.9	0.9	0.9	0.9	0.9	0.4	0.4	0.4	0.4	0.4
Stray light, Fluorescence	0.0	0.0	0.0	0.0	0.0	0.0	0.0	0.0	0.0	0.0
Noise	0.6	0.3	0.6	0.0	0.1	1.4	0.3	1.1	0.0	0.4
Combined uncertainty	3.1	3.0	3.0	3.0	3.1	3.4	3.0	3.7	2.9	3.0
Expanded uncertainty (k=2)	6.3	6.0	6.0	6.0	6.2	6.7	6.1	7.4	5.8	5.9

^aEry, erythematous irradiance

^bDNA, DNA damaging irradiance

^cThe uncertainty due to cosine error is based on clear-sky calculations and may be somewhat larger for scattered-cloud conditions. For overcast conditions, it is 0.5% at all wavelengths and SZAs, see Table 3.

References

- Bernhard G. and G. Seckmeyer (1999), Uncertainty of measurements of spectral solar UV irradiance, *J. Geophys. Res.*, 104(D12), 14,321-14,345.
- Bernhard, G., C. R. Booth, and J. C. Ebrahimian (2004), Version 2 data of the National Science Foundation's Ultraviolet Radiation Monitoring Network: South Pole, *J. Geophys. Res.*, 109, D21207, doi:10.1029/2004JD004937.
- Bernhard, G., C. R. Booth, and J. C. Ebrahimian (2005a), UV climatology at Palmer Station, Antarctica, in: Ultraviolet Ground- and Space-based Measurements, Models, and Effects V, edited by G. Bernhard, J. R. Slusser, J. R. Herman, W. Gao, *Proc. SPIE Int. Soc. Opt. Eng.*, 5886, 588607-1 – 588607-12.
- Bernhard, G., C. R. Booth, and J. C. Ebrahimian. (2005b), Real-time ultraviolet and column ozone from multichannel ultraviolet radiometers deployed in the National Science Foundation's ultraviolet monitoring network. *Optical Engineering*, 44(4), 041011-1 - 041011-12.
- Bernhard, G., C. R. Booth, J. C. Ebrahimian, and V. V. Quang (2006a), NSF Polar Programs UV Spectroradiometer Network 2004-2005 Operations Report Volume 14.0, Biospherical Instruments Inc., San Diego, available at www.biospherical.com/NSF.
- Bernhard G., C. R. Booth, J. C. Ebrahimian, and S. E. Nichol (2006b), UV climatology at McMurdo Station, Antarctica, based on Version 2 data of the National Science Foundation's Ultraviolet Radiation Monitoring Network, *J. Geophys. Res.*, 111, D11201, doi:10.1029/2005JD005857.
- Bernhard, G., C. R. Booth, J. C. Ebrahimian, R. Stone, and E. G. Dutton (2007), Ultraviolet and visible radiation at Barrow, Alaska: Climatology and influencing factors on the basis of version 2 National Science Foundation network data, *J. Geophys. Res.*, 112, D09101, doi:10.1029/2006JD007865.
- International Standards Organization (ISO) (1993), *Guide to the Expression of Uncertainty in Measurements*, ISO, Geneva, Switzerland.

- McKenzie R., J. Badosa, M. Kotkamp, P. Johnston (2005), Effects of the temperature dependence in PTFE diffusers on observed UV irradiances, *Geophys. Res. Lett.*, 32, L06808, doi:10.1029/2004GL022268.
- McKinlay, A. F. and B. L. Diffey (Eds.) (1987), A reference action spectrum for ultraviolet induced erythema in human skin, in: *Commission International de l'Éclairage (CIE), Research Note*, 6(1), 17-22.
- Setlow, R. B. (1974), The wavelength in sunlight effective in producing skin cancer: a theoretical analysis, *Proc. Natl. Acad. Sci. U.S.A.*, 71(9), 3363-3366.
- Walker, J. H., R. D. Saunders, J. K. Jackson, and D. A. McSparron (1987), Spectral irradiance calibrations, NBS Spec. Publ. U.S., 250-20.
- Yoon, H. W., C. E. Gibson, and P. Y. Barnes (2002), Realization of the National Institute of Standards and Technology detector-based spectral irradiance scale, *Appl. Opt.*, 41(28), 5879-5890.